

# Exotic Cooperative Quantum Optics of Moiré Exciton Superlattices

Haowei Xu,<sup>1,2,\*</sup> Wang Yao,<sup>3</sup> and Ju Li<sup>2,4</sup>

<sup>1</sup>*Department of Physics, City University of Hong Kong, Kowloon, Hong Kong SAR, China*

<sup>2</sup>*Department of Nuclear Science and Engineering,  
Massachusetts Institute of Technology, Cambridge, MA 02139, USA*

<sup>3</sup>*New Cornerstone Science Laboratory, Department of Physics,  
The University of Hong Kong, Hong Kong, China*

<sup>4</sup>*Department of Materials Science and Engineering,  
Massachusetts Institute of Technology, Cambridge, MA 02139, USA*

(Dated: March 10, 2026)

The unique properties of two-dimensional moiré systems have been widely studied from many perspectives. However, relatively little work has explored how the *real space* structure of the moiré systems can directly engender novel properties and functionalities. In this work, we exploit the feature that moiré excitons naturally form an ordered superlattice with a lattice constant comparable to the wavelength of the resonant light, which enables intriguing cooperative optical responses. Particularly, we show that the collective moiré exciton states can have either strongly enhanced (superradiant) or suppressed (subradiant) radiative decay rate, depending on their in-plane wavevector. These super- and subradiant states can be efficiently switched by a gate-induced electric field gradient. Moreover, the cooperative transmittance  $T$  of the nanometer-thick moiré system can be switched from  $T \approx 0$  (opaque) to  $T \approx 1$  (transparent) with less than 2 % heterostrain or a  $1^\circ$  adjustment in the twist angle  $\theta$ . These features are robust against non-radiative losses and inhomogeneity, making the moiré system a highly versatile platform for cooperative quantum optics with potential applications in e.g., single photon storage and switching.

**Introduction.** When two-dimensional materials are stacked with small twist angle and/or lattice mismatch, the moiré pattern is formed, which exhibits a wide variety of exotic phenomena, including correlated insulating states, unconventional superconductivity [1, 2], and orbital ferromagnetism [3–5], among many others. The photonic and optoelectronic properties of moiré systems [6, 7], especially those involving moiré excitons [8–10], have also garnered considerable interest [6, 7] with implications in tunable quantum emitters [6, 11], infrared detectors [12], topological excitons [13], etc.

Most previous studies on their optical responses, however, have focused on the properties derived from a *single* localized moiré exciton. One might argue that the total optical response of the moiré superlattice is a simple summation of the responses of each moiré exciton. This viewpoint aligns with conventional treatments of optical responses in condensed-matter systems, where one defines a susceptibility  $\xi$  per unit cell (or unit volume) and obtains the total response by summing over all units, yielding  $N\xi$  or  $V\xi$ , with  $N$  ( $V$ ) the number of unit cells (crystal volume) participating in the light–matter interaction [14].

This approach is generally valid provided that phase matching of different light beams is properly included [14]. Within such a framework, the real-space structure of the system enters only through the overall scaling factors  $N$  or  $V$ , consistent with the common view that reciprocal  $k$ -space structure plays a more central role than real-space structure in condensed-matter physics.

Nevertheless, such a treatment may *not* be adequate for moiré excitons. While the real-space structure of moiré systems is relatively simple (e.g., honeycomb-like), few studies have examined how this structure can have *direct* consequences for their properties [15, 16]. Crucially, for optical responses, the moiré superlattice constant  $a_M$  can be comparable to the resonant wavelength  $\lambda_0$  when the twist angle is  $\theta \lesssim 1^\circ$ . In this regime, moiré excitons can interfere constructively or destructively during light–matter interactions, so their real-space structure may fundamentally reshape the overall optical response, which can be far from the simple summation  $N\xi$ .

The discussions above motivate us to investigate the *cooperative* optical response of the moiré exciton superlattices. Cooperative optical effects have primarily been explored in the context of e.g., artificial atom arrays [17–19], but have rarely been studied in intrinsic condensed-matter systems. Notable cooperative optical effects include collective Lamb shift [20] and the subradiant optical mirror [21]. While isolated atoms benefit from e.g., narrow non-radiative linewidth, it is experimentally challenging to assemble large and perfectly ordered atomic arrays, limiting their practical applicability. In contrast, moiré systems naturally form ordered lattices with unit filling, that is, each lattice site hosts one exciton, an arrangement that is difficult to realize in artificial atomic platforms. Moreover, the moiré superlattice constant  $a_M$  and many other properties can be controlled by the twist angle  $\theta$ . These features make moiré systems highly promising platforms for exploring cooperative quantum optical phenomena and their potential applications.

In the following, we first introduce the properties of single inter-layer moiré excitons, emphasizing their spa-

\* haoweixu@cityu.edu.hk

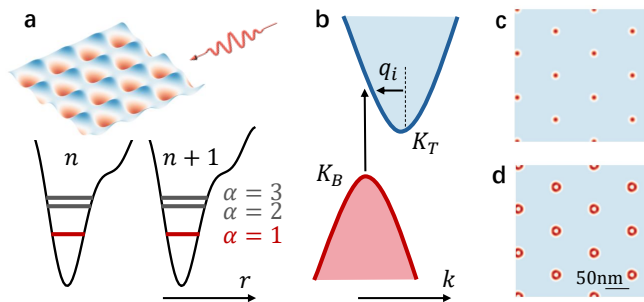


FIG. 1. (a) moiré potential and exciton lattice in real space. Upper panels shows a two-dimensional moiré potential landscape. Lower panel shows multiple localized moiré exciton states in each potential minimum, labeled by  $\alpha$ . In this work, we focus on the lowest energy  $\alpha = 1$  state. (b) Illustration of the electronic band structure of the moiré system in the unfolded Brillouin zone. The electron acquires a wave vector  $q_i$  relative to  $K_T$  after vertical optical transition from  $K_B$ . (c, d) Real space wavefunction  $|\langle r | \chi_\alpha \rangle|$  of (a)  $\alpha = 1$  and (b)  $\alpha = 2$  exciton with  $\theta = 0.2^\circ$ . Blue (red) color denotes small (large) wavefunction amplitude.

tial localization and optical responses. We then explore several significant cooperative quantum optical effects of moiré exciton superlattices. Particularly, we show that collective moiré exciton states can have extremely high (superradiant) or low (subradiant) radiative decay rate, depending on their in-plane wavevector. The subradiant states can have lifetimes extended by orders of magnitude compared with a single exciton, making them promising candidates for photon memory [22, 23]. Additionally, an gate-induced electric field gradient can dynamically switch the system between superradiant and subradiant states, enabling efficient photon storage and retrieval. We further demonstrate that the light transmittance  $T$  of a moiré exciton superlattice can be tuned from  $T \approx 1$  to  $T \approx 0$ , with less than 2% heterostrain or  $1^\circ$  change in the twist angle, allowing the system to function as an efficient single photon switch [24]. These properties remain robust against non-radiative losses and inhomogeneous broadening up to a few hundred GHz, well within experimental reach given that the overall linewidth of moiré excitons can be as narrow as 20 GHz [9].

**Properties of moiré excitons.** Firstly, we briefly introduce the properties of single moiré excitons, focusing on their spatial localization and optical transition dipole moments, which are most relevant to their cooperative optical responses. Detailed discussions can be found in the Supplementary Materials (SM) Sections 1-3. Without loss of generality, we assume the top and bottom layers are 2H phase MoS<sub>2</sub> and WS<sub>2</sub> with AA stacking [11, 13]

Without the moiré potential, a free exciton state can be labelled by  $|Q\rangle$ , with total momentum  $Q$  and total energy  $\hbar\omega_0 + \frac{\hbar Q^2}{2M}$ . Here,  $\hbar\omega_0$  is the energy of an exciton with  $Q = 0$  and is typically on the order of  $1 \sim 2$  eV [25].

Meanwhile,  $\frac{\hbar Q^2}{2M}$  is the kinetic energy of the exciton with  $M$  the total mass of the electron and hole. Notably,  $|Q\rangle$  are delocalized plane-wave-like states, meaning that the exciton center-of-mass coordinate  $r$  has a simple spatial profile  $Q(r) \sim e^{iQ \cdot r}$ . The optical transition dipole between the ground state  $|G\rangle$  and  $|Q\rangle$  is nonzero only when  $Q = q_i$  ( $i = 1, 2, 3$ ), where  $q_1 = K_T - K_B$ , while  $q_2$  and  $q_3$  are obtained from  $q_1$  by  $2\pi/3$  and  $4\pi/3$  rotations, respectively. Here  $K_T$  and  $K_B$  are the  $K$ -valley of the top and bottom layer (Figure 1b and Figure S2 in SM). This selection rule follows from momentum conservation in optical transitions. Because the photon momentum is negligible, an electron initially at  $K_B$  acquires a wavevector of  $q_i$  relative to  $K_T$  after a vertical optical transition (Figure 1b).

The moiré structure leads to a potential field  $\Delta(r)$  for the excitons, which has the same periodicity as the moiré superlattice and breaks the original translational symmetry (Figure 1a). This results in the hybridization between free exciton states, namely  $\langle Q | \Delta(r) | Q' \rangle = \sum_{n=1}^6 V_n \delta_{Q, Q' + b_n}$ , where  $\delta$  is the Kronecker delta,  $b_n$  are the moiré reciprocal lattice vectors, and  $V_n$  characterizes the depth of the moiré potential, which is typically tens of meV for inter-layer excitons [11, 13]. The new moiré exciton eigenstates are  $|\chi_{\alpha, Q}\rangle = \sum_{Q'} f_{QQ'}^\alpha |Q'\rangle$ . Here,  $Q$  is restricted to the first Brillouin zone of the moiré superlattice, while the summation over  $Q'$  is limited to those connected to  $Q$  by  $b_n$ . Note that  $Q$ -points outside the first moiré Brillouin zone are folded back into it, giving rise to an additional band index  $\alpha$ , which labels the moiré exciton states on each  $Q$ -point in order of increasing energy. The energy difference between different  $\alpha$  states is on the order of meV (Figure 1a, SM Section 2). This is analogous to the formation of electron bands in the nearly free electron model [26]. The optically bright momenta  $Q = q_1, q_2, q_3$  are hybridized by  $\Delta(r)$  and are equivalent due to the three-fold rotational symmetry of the system. The moiré exciton eigenstates have equivalent contributions from the  $Q = q_1, q_2, q_3$  modes and therefore have a total momentum of zero. Their optical responses can be derived from those of the  $|\chi_{\alpha, Q=q_1}\rangle$  mode. In the following, we focus on the optically bright  $\alpha = 1$  mode, and use the shorthand  $|\chi\rangle$  to denote this optically bright exciton unless otherwise noted.

Next, we consider the spatial profile of the moiré exciton. The real space wavefunction, expressed as  $\langle r | \chi \rangle = \sum_{Q'} f_{QQ'} e^{iQ' \cdot r}$ , are localized at the minima of the moiré potential (Figure 1c, 1d). For further discussions, one can define approximate exciton wave packets  $|R\rangle = \sum_{Q'} W(Q') |Q'\rangle$ , mimic an exciton localized at the lattice site  $R$  with a proper choice of  $W(Q')$ . The  $\alpha = 1$  exciton has a  $s$ -wave profile and can be represented by an isotropic envelope  $W(Q') = \sqrt{4\pi/S} w e^{-w^2 |Q'|^2 / 2}$ , where  $S$  is a normalization area. Notably, the width  $w$  of the moiré exciton wavefunction is on the order of a few nanometers, much smaller than the optical wavelength, which is hundreds of nanometers. Therefore, each localized moiré exciton can be treated as a point-like dipole in

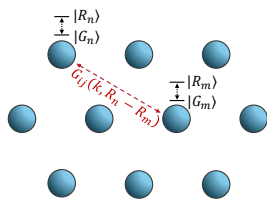


FIG. 2. An ordered moiré superlattice. Each lattice site  $R_n$  is modeled by a two-level system  $|R_n\rangle$  and  $|G_n\rangle$ . The red arrow indicates the interactions among moiré excitons, characterized by the Green's function  $G_{ij}$ .

optical response calculations. This significantly simplifies the analyses on their cooperative optical response.

The width of the wave packet  $w$  is also crucial in the optical transitions. Particularly, the optical transition dipole moment  $d \equiv \langle G | \hat{d} | R \rangle$  is proportional to  $w$ . Here  $\hat{d}$  is the dipole operator and  $|G\rangle$  is the ground state, i.e., no excitons at this lattice point. The property of  $d \propto w$  is similar to the optical transition dipoles of quantum dots, which scale linearly with their size [27]. For a wide range of twist angle, one has  $w \sim 0.3a_M \propto 1/\theta$ . Hence, we adopt  $d \approx \frac{d_0}{\theta}$  with  $d_0 = 0.1 e \cdot \text{\AA}$ . As  $d$  increases for larger  $a_M$  (smaller  $\theta$ ), the dipole-dipole interaction among moiré excitons can remain strong even if  $a_M$  is large (SM Section 2).

Strictly speaking, excitons are bosons, so multiple excitons can in principle occupy the same potential minimum. However, if more than one exciton occupies the same site, then the on-site exciton-exciton interactions would introduce a resonance frequency shift [11] (analogous to the Hubbard  $U$  for electrons), much larger than the energy scale relevant here. Hence, when the incident light is (nearly) resonant with the transition between  $|G\rangle$  (no exciton) and  $|R\rangle$  (one exciton), states with multiple excitons are far off-resonance and can be neglected.

In short, we model exciton on each superlattice site as a two-level system with states  $|G\rangle$  and  $|R\rangle$  and transition dipole moment  $d$ . This picture will be used in the following sections (Figure 2).

**Interactions among moiré excitons.** In the previous section, we focused on the properties of a single moiré exciton. Now we turn to the ordered superlattice formed by  $N$  moiré excitons. We will a subscript  $n$  to denote an exciton at lattice site  $R_n$  (Figure 2).

These localized moiré excitons interact with one another through dipole-dipole interactions, and the interaction between two excitons at locations  $R_n$  and  $R_m$  can be described by the Green's function

$$G_{ij}(k, r) = \frac{e^{ikr}}{4\pi k^2 r^3} [(k^2 r^2 + ikr - 1)\delta_{ij} + (-k^2 r^2 - 3ikr + 3)\frac{r_i r_j}{r^2}] \quad (1)$$

where we defined  $r = R_n - R_m$ .  $i, j$  are Cartesian indices, and  $\delta_{ij}$  is the Kronecker delta. The vacuum Green's function [28] is used for simplicity.  $k$  is the wavevector of

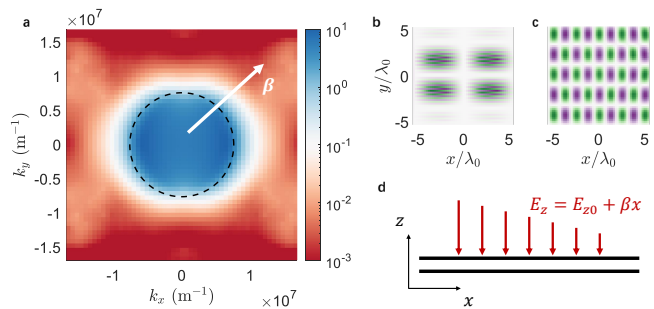


FIG. 3. (a) Collective radiative decay rate  $\Gamma_\nu$  as a function of in-plane wavevector  $k_\parallel$  for a finite lattice with approximately  $50 \times 50$  excitons. The dashed circle denotes the light cone with  $|k_\parallel| = k_0$ . (b, c) Real part of the wavefunction of the collective exciton in real space, i.e.,  $\text{Re}[\langle R_n | \nu(k_\parallel) \rangle]$ . (b) and (c) correspond to two states with  $|k_\parallel| > k_0$  and  $|k_\parallel| < k_0$ . Each pixel corresponds to moiré lattice site  $R_n$ . Blue (purple) color indicate positive (negative) values of the wavefunction. (d) A collective exciton state can be switched between super- to sub-radiant states by an electric field gradient  $\beta$ . The electric field is along out-of-plane  $z$  direction, while the gradient is along the in-plane  $x$  or  $y$  direction.

the electromagnetic field. Note that Eq. (1) is a formal solution of the Maxwell equation and captures all possible interactions between two dipoles. In the far field  $kr \gg 1$ ,  $G$  reduces to the standard dipole radiation, scaling as  $G \sim e^{ikr}/r$ . In the static limit ( $k = 0$ ), it reproduces the familiar dipole-dipole interaction that scales as  $1/r^3$ . Moreover, for the self-interaction of a single exciton ( $R_n = R_m$ ), its radiative decay rate is given by  $\gamma_0 \propto \text{Im}[G(k, r \rightarrow 0)]$ .

The interactions among dipoles, encoded in the Green's function, can lead to exotic cooperative effects, as we will discuss below.

**Superradiant and subradiant states.** We will first discuss super- and sub-radiance of the collective moiré exciton states [18, 29, 30] and how they can be dynamically switched, providing a mechanism for light storage and retrieval.

The total Hamiltonian of the exciton lattice can be expressed as [18]

$$H_{\text{eff}} = \hbar\omega_0 \sum_{n=1}^N |R_n\rangle\langle R_n| + \frac{\omega_0^2 d^2}{\varepsilon_0 c_0^2} \sum_{m,n=1}^N G_{xx}(k_0, R_n - R_m) |G_n\rangle\langle R_n| \otimes |R_m\rangle\langle G_m| \quad (2)$$

The first term is the non-interacting Hamiltonian with exciton energy  $\omega_0$ . It is zero if a lattice site is on  $|G_n\rangle$  and is  $\hbar\omega_0$  if on  $|R_n\rangle$ . Meanwhile, the second term of Eq. (2) describes the long-range dipole-dipole interaction among moiré excitons. Here,  $\varepsilon_0$  and  $c_0$  are the vacuum permittivity and speed of light, respectively, and we define  $k_0 = \omega_0/c_0$ . The transition dipole  $d$  is assumed to be the same for all excitons. We do not include the out-

of-plane permanent dipole  $d_z \equiv \langle R_n | \hat{d} | R_n \rangle$  of the interlayer exciton, as it is much smaller than  $d$  [11]. Without loss of generality, we consider excitons excited by light polarized along the  $x$ -direction, so only  $G_{xx}$  appears in Eq. (2). The full  $H_{\text{eff}}$  has a dimension of  $2^N$ , but we focus on the single-excitation sub-space spanned by the basis  $|\psi^n\rangle \equiv |G_1 G_2, \dots, R_n, \dots, G_N\rangle, n = 1, 2, \dots, N$ , whose dimension is  $N$ .

The effective Hamiltonian  $H_{\text{eff}}$  is non-Hermitian. Nevertheless, one can still investigate its eigenstates  $|\nu\rangle$  with complex eigenvalues  $J_\nu - i\frac{\Gamma_\nu}{2}$ . Here,  $J_\nu$  and  $\Gamma_\nu$  correspond to the collective lineshift and radiative decay rate, respectively. While the Hamiltonian in Eq. (2) does not include kinetic propagation of moiré excitons, assuming that they are well trapped in the moiré landscapes, the dipole Green's function does account for Forster type non-radiative coupling that allows moiré excitons to effectively hop between the trapping sites [16]. Generally,  $|\nu\rangle$  are collective exciton states, similar to the Bloch functions, and  $|\langle \psi_n | \nu \rangle|^2$  is the probability of finding the exciton at lattice site  $R_n$ . For an infinite exciton lattice,  $|\nu\rangle$  can be labeled by the in-plane wavevector  $k_{\parallel}$ , according to Bloch's theorem. That is, one has  $|\nu(k_{\parallel})\rangle \propto \sum_n e^{ik_{\parallel} \cdot R_n} |\psi_n\rangle$ . Notably, for  $k_{\parallel} > k_0$ , one has  $\Gamma_\nu = 0$ , and the excitons are completely dark (SM Section 4). For  $k_{\parallel} < k_0$ , superradiance  $\Gamma_\nu > \gamma_0$  typically occurs. This superradiance-subradiance transition arises from the momentum conservation: the in-plane momentum  $k_{\parallel}$  of the emitted photon must match that of the collective exciton. For  $k_{\parallel} > k_0$ , the out-of-plane wavevector  $\sqrt{k_0^2 - k_{\parallel}^2}$  becomes imaginary, producing an evanescent field and suppressing radiation ( $\Gamma_\nu = 0$ ).

In practice, the moiré exciton lattice is finite, and one cannot assign a definite  $k_{\parallel}$  to each eigenstate. We numerically diagonalize  $H_{\text{eff}}$  for a  $50 \times 50$  exciton lattice. Selected wavefunctions  $|\nu\rangle$  are plotted in Figures 3b, 3c. These states exhibit semi-periodic patterns, allowing for a Fourier transform to extract the dominant  $k_{\parallel}$  component, which can be used to label  $|\nu\rangle$  as  $\langle \psi_n | \nu(k_{\parallel}) \rangle \approx e^{ik_{\parallel} \cdot R_n}$ . Using this approach, we obtained the  $\Gamma_\nu$ - $k_{\parallel}$  relationship (Figure 3a). Notably, there is still a transition from superradiance ( $\Gamma_\nu \gg \gamma_0$ ) to subradiance ( $\Gamma_\nu \ll \gamma_0$ ) at the light cone boundary  $|k_{\parallel}| = k_0$ . The transition is smooth due to the finite-size effect, and states with  $|k_{\parallel}| < k_0$  are not entirely dark - their  $\Gamma_\nu$  is small but non-zero.

**Switching between superradiant and subradiant states.** A collective exciton state excited by an external photon must have  $k_{\parallel} < k_0$  and is therefore superradiant. This allows the photon to be efficiently transferred into an exciton state. For long-term photon storage, however, the excitation should reside in a subradiant state, which has a much longer lifetime.

Hence, effective light storage and retrieval requires controllable switching between superradiant and subradiant states. This can be achieved by applying a gate electric field with a spatial gradient, which leads to a Hamilto-

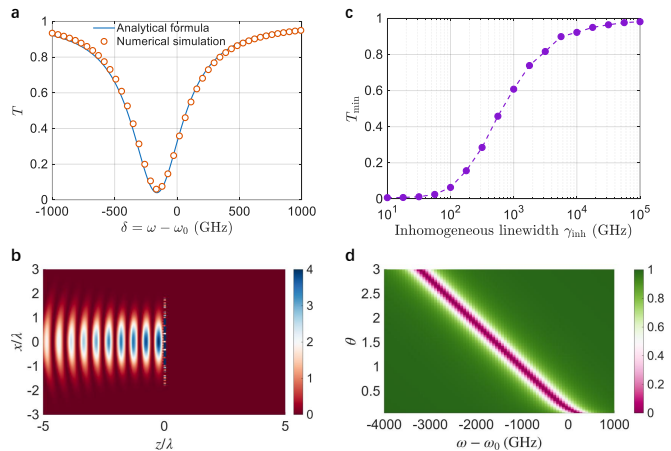


FIG. 4. (a) Transmittance  $T(\omega)$  as a function of frequency detuning  $\omega - \omega_0$  with  $\theta = 0.2^\circ$ . (b) The electric field profile  $|E(r)|^2$  at  $\omega - \omega_0 \approx 161$  GHz, where  $T(\omega)$  reaches the minimum at  $\theta = 0.2^\circ$ . Light is incident from left, and the fields  $|E(r)|^2$  are normalized by  $E_0^2$  with  $E_0$  the incident field strength. (c) Minimum of  $T$  as a function of inhomogeneous linewidth with  $\theta = 0.2^\circ$ . (d)  $T$  as a function of  $\omega - \omega_0$  for varied  $\theta$ . The non-radiative linewidth is taken as  $\gamma_{\text{nr}} = 100$  GHz in these plots.

nian  $H_\beta = \sum_n d_z \cdot \beta \cdot R_n |R_n\rangle \langle R_n|$ , where  $d_z = \langle R_n | \hat{d} | R_n \rangle$  is the out-of-plane dipole of the exciton. This electric field is along the  $z$  direction, while the gradient  $\beta$  lies in-plane (along  $x$  or  $y$  in Figure 3d).  $H_\beta$  induces a position-dependent phase, effectively shifting the exciton wavevector, namely [31]

$$k_{\parallel} \rightarrow k_{\parallel} + \frac{d_z \cdot \beta}{\hbar} \tau, \quad (3)$$

with the  $\tau$  the duration of the applied electric field gradient. With a suitable  $\tau$ , a superradiant exciton can be pushed beyond the light-cone and become subradiant. In practice, this can be achieved within nanoseconds with  $\beta \sim 10^{10}$  V/m<sup>2</sup>. To restore the superradiant state, one can simply reverse the direction of the electric field ( $-\beta$ ) for the same duration  $\tau$ . Note that  $\beta$  does not need to be uniform in real space.

Intuitively, Eq. (3) resembles the semiclassical equation of motion for an electron in a crystal,  $k \rightarrow k + eE\tau/\hbar$ , where the electron charge  $e$  couples directly to the electric field  $E$ . In contrast, an exciton carries no net charge but only a dipole moment  $d_z$ , so its wavevector can be modified only via the electric-field gradient  $\beta$ .

**Cooperative photon scattering.** Besides photon absorption and emission, cooperative optical effects also appear in photon scattering. As an example, we study the transmittance  $T$  of the moiré exciton lattice. Intuitively, few-layer 2D materials should have  $T \approx 1$ , as they are too thin to significantly reflect or absorb light. For example, monolayer graphene has  $T \approx 0.97$  [32]. Remarkably, as we show below, the moiré exciton lattice can exhibit nearly zero transmittance.

Assuming an incident field  $E_0(r)$  with frequency  $\omega$  and wavelength  $\lambda$ , the total field  $E(r)$  satisfies [17, 19, 33]

$$E_i(r) = E_{0,i}(r) + \frac{4\pi^2\alpha}{\varepsilon_0\lambda^2} \sum_{jn} G_{ij}(k, r - R_n) E_j(R_n) \quad (4)$$

where  $i, j = x, y, z$ . For simplicity, we consider  $x$ -polarized light incident normally along  $z$  onto the exciton lattice plane ( $x$ - $y$  plane), though other geometries can be analyzed similarly. Eq. (4) indicates that the total field  $E(r)$  is the sum of the incident field  $E_0(r)$  and the field scattered by the exciton dipole at  $R_n$ , mediated by the propagator  $G_{ij}(k, r - R_n)$ . The exciton polarizability is  $\alpha(\omega) = \frac{2d^2\omega_0}{\hbar} \frac{1}{\omega_0^2 - \omega^2 - i\gamma\omega}$ . The total linewidth of a single exciton is given by  $\gamma = \gamma_r + \gamma_{nr}$ , where  $\gamma_r$  and  $\gamma_{nr}$  are the radiative and non-radiative components, respectively. Each moiré exciton may also experience an inhomogeneous shift in its resonance frequency  $\omega_0$ , characterized by an inhomogeneous linewidth  $\gamma_{inh}$ .

We first numerically study a finite exciton lattice with  $\theta = 0.2^\circ$  ( $a_M \approx 0.11\lambda_0$ ) with  $\gamma_{nr} = 100$  GHz and  $\gamma_{inh} = 0$  (details in SM Section 5). The transmittance  $T$  versus frequency detuning  $\delta = \omega - \omega_0$  is plotted in Figure 4a. Intriguingly, nearly zero transmission appears at  $\delta \approx -161$  GHz. The field profile (Figure 4b) shows that the scattered field and the incident field form a standing wave in the  $z < 0$  region. In the  $z > 0$  region, the two fields add destructively, leading to zero transmission (SM Section 5.1).

Analytically, for an infinite exciton lattice with  $a_M < \lambda$ , one has (SM Section 5.2) [33]

$$T(\omega) = \left| 1 - \frac{\frac{i}{2} \left( \frac{\lambda_0^3}{\lambda^3} \gamma_0 + \Gamma \right)}{\omega - \omega_0 + \Delta + \frac{i}{2} (\gamma_0 + \gamma_{nr} + \Gamma)} \right|^2, \quad (5)$$

where the collective lineshift  $\Delta$  and the collective radiative decay rate  $\Gamma$  are

$$\Delta = \frac{3\gamma_0 \lambda_0^3}{2 \lambda^3} \lambda \text{Re}\{\mathcal{G}_{xx}(0)\}, \quad \Gamma = \frac{3\gamma_0 \lambda_0^3 \lambda^2}{4\pi \lambda^3 A} - \frac{\lambda_0^3}{\lambda^3} \gamma_0, \quad (6)$$

with  $\mathcal{G}_{xx}(0) = \sum_{n \neq 0} G_{xx}(k, R_n)$  and  $A$  the area of the moiré superlattice. Intuitively, the moiré excitons interact cooperatively [Eq. (1) and Figure 2], forming a collective excitation that behaves like a giant atom. Zero transmittance occurs at the collective resonance  $\Delta + \omega - \omega_0 = 0$  when  $\gamma_{nr} = 0$ , which is demonstrated in Figure 4d for varied  $\theta$ .

Notably, this cooperative effect is robust to inhomogeneity  $\gamma_{inh}$  and non-radiative damping  $\gamma_{nr}$ , provided that they remain below the *collective* radiative decay rate  $\Gamma$  [cf. Eq. (5)]. Our results indicate that transmittance below 0.2 can be realized with  $\gamma_{inh}, \gamma_{nr} \lesssim 100$  GHz (Figure 4c and SM Section 5.3).

More importantly, this effect is highly sensitive to the twist angle  $\theta$  (Figure 4d), enabling an efficient light switch. At a fixed light frequency, nearly zero transmission  $T \approx 0$  and full transmission  $T \approx 1$  can be toggled by varying  $\theta$  by less than  $1^\circ$ . This is because the collective shift  $\Delta$  strongly depends on the moiré lattice spacing, which is controlled by the twist angle. From this perspective, a heterostrain  $u$  can also be used to turn  $T$ . This is because the moiré superlattice constant scales as  $a_M \propto \frac{1}{\sqrt{u^2 + \theta^2}}$ . Therefore, applying heterostrain is effectively equivalent to tuning  $\theta$  in terms of modify  $a_M$ . Using heterostrain, one can realize in situ and reversible control over  $T$ .

**Discussions and conclusions.** It is well-known that the optical response of an atom is strongly influenced by its electromagnetic environment. For example, an optical cavity can modify the atomic radiative decay through the Purcell effect [34], and single photon switching be achieved with atoms in nanophotonic platforms [35–37]. From this perspective, in a moiré exciton lattice, the local electromagnetic environment experienced by each exciton is set by its neighboring excitons. An exciton A can (virtually) transfer its excitation to surrounding excitons and receive it back [16], meaning that neighboring excitons effectively act as a resonator for exciton A [38]. In this sense, the moiré exciton lattice parallels a single atom coupled to a nanophotonic structure, thereby enabling the cooperative quantum optical functionalities discussed above.

These cooperative optical responses require moiré excitons to have linewidths below a few hundred GHz. Fortunately, linewidths as narrow as tens of GHz have been reported at a few Kelvin [9]. In non-moiré two-dimensional materials, exciton lifetimes can even reach the microsecond range [39], and the cooperative coupling and superradiance of excitons have been experimental observed [40, 41]. Therefore, cooperative quantum optics with moiré exciton superlattices, as proposed here, should be experimentally feasible with high-quality, low-inhomogeneity samples. The moiré superlattice thus provides a versatile platform for exploring both fundamental cooperative many-body quantum optics and potential applications in photonics and optoelectronics, all at the two-dimensional limit.

[1] Yuan Cao, Valla Fatemi, Shiang Fang, Kenji Watanabe, Takashi Taniguchi, Efthimios Kaxiras, and Pablo Jarillo-Herrero, “Unconventional superconductivity in magic-angle graphene superlattices,” *Nature* **556**, 43–50 (2018).

[2] Yuan Cao, Valla Fatemi, Ahmet Demir, Shiang Fang, Spencer L Tomarken, Jason Y Luo, Javier D Sanchez-Yamagishi, Kenji Watanabe, Takashi Taniguchi, Efthimios Kaxiras, *et al.*, “Correlated insulator be-

- haviour at half-filling in magic-angle graphene superlattices,” *Nature* **556**, 80–84 (2018).
- [3] Aaron L Sharpe, Eli J Fox, Arthur W Barnard, Joe Finney, Kenji Watanabe, Takashi Taniguchi, MA Kastner, and David Goldhaber-Gordon, “Emergent ferromagnetism near three-quarters filling in twisted bilayer graphene,” *Science* **365**, 605–608 (2019).
  - [4] Guorui Chen, Aaron L Sharpe, Eli J Fox, Ya-Hui Zhang, Shaoxin Wang, Lili Jiang, Bosai Lyu, Hongyuan Li, Kenji Watanabe, Takashi Taniguchi, *et al.*, “Tunable correlated chern insulator and ferromagnetism in a moiré superlattice,” *Nature* **579**, 56–61 (2020).
  - [5] M Serlin, CL Tschirhart, H Polshyn, Y Zhang, J Zhu, K Watanabe, T Taniguchi, L Balents, and AF Young, “Intrinsic quantized anomalous hall effect in a moiré heterostructure,” *Science* **367**, 900–903 (2020).
  - [6] Hyeonjun Baek, Mauro Brotons-Gisbert, Zhe Xian Koong, Aidan Campbell, Markus Rambach, Kenji Watanabe, Takashi Taniguchi, and Brian D Gerardot, “Highly energy-tunable quantum light from moiré-trapped excitons,” *Science advances* **6**, eaba8526 (2020).
  - [7] LuoJun Du, Maciej R Molas, Zhiheng Huang, Guangyu Zhang, Feng Wang, and Zhipei Sun, “Moiré photonics and optoelectronics,” *Science* **379**, eadg0014 (2023).
  - [8] Kha Tran, Galan Moody, Fengcheng Wu, Xiaobo Lu, Junho Choi, Kyoungwan Kim, Amritesh Rai, Daniel A Sanchez, Jiamin Quan, Akshay Singh, *et al.*, “Evidence for moiré excitons in van der waals heterostructures,” *Nature* **567**, 71–75 (2019).
  - [9] Kyle L Seyler, Pasqual Rivera, Hongyi Yu, Nathan P Wilson, Essance L Ray, David G Mandrus, Jiaqiang Yan, Wang Yao, and Xiaodong Xu, “Signatures of moiré-trapped valley excitons in mose2/wse2 heterobilayers,” *Nature* **567**, 66–70 (2019).
  - [10] Chenhao Jin, Emma C Regan, Aiming Yan, M Iqbal Bakti Utama, Danqing Wang, Sihan Zhao, Ying Qin, Sijie Yang, Zhiren Zheng, Shenyang Shi, *et al.*, “Observation of moiré excitons in wse2/ws2 heterostructure superlattices,” *Nature* **567**, 76–80 (2019).
  - [11] Hongyi Yu, Gui-Bin Liu, Jianju Tang, Xiaodong Xu, and Wang Yao, “Moiré excitons: From programmable quantum emitter arrays to spin-orbit-coupled artificial lattices,” *Science advances* **3**, e1701696 (2017).
  - [12] Chao Ma, Shaofan Yuan, Patrick Cheung, Kenji Watanabe, Takashi Taniguchi, Fan Zhang, and Fengnian Xia, “Intelligent infrared sensing enabled by tunable moiré quantum geometry,” *Nature* **604**, 266–272 (2022).
  - [13] Fengcheng Wu, Timothy Lovorn, and Allan H MacDonald, “Topological exciton bands in moiré heterojunctions,” *Physical review letters* **118**, 147401 (2017).
  - [14] Yuen-Ron Shen, “Principles of nonlinear optics,” (1983).
  - [15] Haochen Wang and Wang Yao, “Emergent kagome lattice and non-abelian lattice gauge field of biexcitons in t-mote2,” *National Science Review* **13**, nwaf328 (2026).
  - [16] Huiyuan Zheng, Ci Li, Hongyi Yu, and Wang Yao, “Förster valley-orbit coupling and topological lattice of hybrid moiré excitons,” *Communications Physics* **8**, 193 (2025).
  - [17] Robert J Bettles, Simon A Gardiner, and Charles S Adams, “Enhanced optical cross section via collective coupling of atomic dipoles in a 2d array,” *Physical review letters* **116**, 103602 (2016).
  - [18] Ana Asenjo-Garcia, M Moreno-Cardoner, Andreas Albrecht, HJ Kimble, and Darrick E Chang, “Exponential improvement in photon storage fidelities using subradiance and selective radiance in atomic arrays,” *Physical Review X* **7**, 031024 (2017).
  - [19] Ephraim Shahmoon, Dominik S Wild, Mikhail D Lukin, and Susanne F Yelin, “Cooperative resonances in light scattering from two-dimensional atomic arrays,” *Physical review letters* **118**, 113601 (2017).
  - [20] Antoine Glicenstein, Giovanni Ferioli, Nikola Šibalić, Ludovic Brossard, Igor Ferrier-Barbut, and Antoine Browaeys, “Collective shift in resonant light scattering by a one-dimensional atomic chain,” *Physical Review Letters* **124**, 253602 (2020).
  - [21] Jun Rui, David Wei, Antonio Rubio-Abadal, Simon Hollerith, Johannes Zeiher, Dan M Stamper-Kurn, Christian Gross, and Immanuel Bloch, “A subradiant optical mirror formed by a single structured atomic layer,” *Nature* **583**, 369–374 (2020).
  - [22] Sheng Zhang, Jixuan Shi, Zhaibin Cui, Ye Wang, Yukai Wu, Luming Duan, and Yunfei Pu, “Realization of a programmable multipurpose photonic quantum memory with over-thousand qubit manipulations,” *Physical Review X* **14**, 021018 (2024).
  - [23] Yu-Ping Liu, Zhong-Wen Ou, Tian-Xiang Zhu, Ming-Xu Su, Chao Liu, Yong-Jian Han, Zong-Quan Zhou, Chuan-Feng Li, and Guang-Can Guo, “A millisecond integrated quantum memory for photonic qubits,” *Science Advances* **11**, eadu5264 (2025).
  - [24] Shuo Sun, Hyochul Kim, Zhouchen Luo, Glenn S Solomon, and Edo Waks, “A single-photon switch and transistor enabled by a solid-state quantum memory,” *Science* **361**, 57–60 (2018).
  - [25] Gang Wang, Alexey Chernikov, Mikhail M Glazov, Tony F Heinz, Xavier Marie, Thierry Amand, and Bernhard Urbaszek, “Colloquium: Excitons in atomically thin transition metal dichalcogenides,” *Reviews of Modern Physics* **90**, 021001 (2018).
  - [26] Charles Kittel and Paul McEuen, *Introduction to solid state physics* (John Wiley & Sons, 2018).
  - [27] Lucjan Jacak, Pawel Hawrylak, and Arkadiusz Wojs, *Quantum dots* (Springer Science & Business Media, 2013).
  - [28] Lukas Novotny and Bert Hecht, *Principles of nano-optics* (Cambridge university press, 2012).
  - [29] Robert H Dicke, “Coherence in spontaneous radiation processes,” *Physical review* **93**, 99 (1954).
  - [30] Stuart J Masson, Igor Ferrier-Barbut, Luis A Orozco, Antoine Browaeys, and Ana Asenjo-Garcia, “Many-body signatures of collective decay in atomic chains,” *Physical review letters* **125**, 263601 (2020).
  - [31] David Plankensteiner, Laurin Ostermann, Helmut Ritsch, and Claudiu Genes, “Selective protected state preparation of coupled dissipative quantum emitters,” *Scientific reports* **5**, 16231 (2015).
  - [32] Shou-En Zhu, Shengjun Yuan, and GCAM Janssen, “Optical transmittance of multilayer graphene,” *Europhysics Letters* **108**, 17007 (2014).
  - [33] Francisco Javier Garcia de Abajo, “Colloquium: Light scattering by particle and hole arrays,” *Reviews of modern physics* **79**, 1267–1290 (2007).
  - [34] Edward Mills Purcell, “Spontaneous emission probabilities at radio frequencies,” in *Confined electrons and photons: new physics and applications* (Springer, 1995) pp. 839–839.
  - [35] TG Tiecke, Jeffrey Douglas Thompson, Nathalie Pul-

- mones de Leon, LR Liu, Vladan Vuletić, and Mikhail D Lukin, “Nanophotonic quantum phase switch with a single atom,” *Nature* **508**, 241–244 (2014).
- [36] Itay Shomroni, Serge Rosenblum, Yulia Lovsky, Orel Bechler, Gabriel Guendelman, and Barak Dayan, “All-optical routing of single photons by a one-atom switch controlled by a single photon,” *Science* **345**, 903–906 (2014).
- [37] Alp Sipahigil, Ruffin E Evans, Denis D Sukachev, Michael J Burek, Johannes Borregaard, Mihir K Bhaskar, Christian T Nguyen, Jose L Pacheco, Haig A Atikian, Charles Meuwly, *et al.*, “An integrated diamond nanophotonics platform for quantum-optical networks,” *Science* **354**, 847–850 (2016).
- [38] Raphael Holzinger, David Plankensteiner, Laurin Ostermann, and Helmut Ritsch, “Nanoscale coherent light source,” *Physical Review Letters* **124**, 253603 (2020).
- [39] Luis A Jauregui, Andrew Y Joe, Kateryna Pistunova, Dominik S Wild, Alexander A High, You Zhou, Giovanni Scuri, Kristiaan De Greve, Andrey Sushko, Che-Hang Yu, *et al.*, “Electrical control of interlayer exciton dynamics in atomically thin heterostructures,” *Science* **366**, 870–875 (2019).
- [40] Jason Horng, Yu-Hsun Chou, Tsu-Chi Chang, Chu-Yuan Hsu, Tien-Chang Lu, and Hui Deng, “Engineering radiative coupling of excitons in 2d semiconductors,” *Optica* **6**, 1443–1448 (2019).
- [41] Golam Haider, Krishna Sampathkumar, Tim Verhagen, Lukas Nadvornik, Farjana J Sonia, Vaclav Vales, Jan Sykora, Peter Kapusta, Petr Nemeč, Martin Hof, *et al.*, “Superradiant emission from coherent excitons in van der waals heterostructures,” *Advanced Functional Materials* **31**, 2102196 (2021).